# Light-shift-induced chaos in a nonlinear optical resonator

C. Boden, M. Dämmig, and F. Mitschke
*Institut für Quantenoptik, Universität Hannover, Welfengarten 1, D-3000 Hannover 1, Germany*
(Received 28 August 1991; revised manuscript received 4 December 1991)

The interaction of spin-$\frac{1}{2}$ atoms in an optical resonator with a near-resonant cw light field and an external static magnetic field gives rise to self-sustained spin precession. This entails a modulation on the transmitted light at roughly the Larmor frequency. We show that under suitable conditions this oscillation can become irregular. A detailed analysis reveals a deterministically chaotic process. Dimensions, entropies, and Lyapunov exponents are determined; cross-checks demonstrate their mutual consistency. To describe the observed dynamics, a three-dimensional model is presented that resembles the well-known Bloch equations. Numerical simulations compare well with the experimental results. Of all the nonlinear terms in the model, the one describing the light shift can be singled out as responsible for the chaotic behavior. This allows an intuitive understanding of the onset of chaos as a result of the interaction between spin precession and light shift.

PACS number(s): 42.50.Lc, 32.80.−t

## I. INTRODUCTION

Complex dynamic behavior can arise from fairly simple structures. Nonlinear systems with a mere three degrees of freedom can, e.g., exhibit chaotic oscillations. Unfortunately, there are few general mathematical theorems by which one can determine the types of behavior a given system is capable of. It is hoped that the pattern of just what the precise conditions for chaos are will soon emerge. Meanwhile, it is important that in various experiments the physical mechanism of the generation of chaos is well understood.

Chaotic dynamics has been studied in many fields [1,2]. The field of quantum optics is no exception, and in particular, lasers of various kinds (single or multimode, with homogeneously or inhomogeneously broadened gain media, with saturable absorbers, etc.) have been researched extensively [3–8].

Passive systems, on the other hand, can display dynamic behavior which is just as rich and interesting [6–8]. They also come with the additional bonus that the presence of an external light field with fixed frequency precludes some of the complications met in active systems such as mode shifting, etc.

In this contribution, chaos in a passive optical cavity is shown to be caused by the light shift, the shift of atomic levels that arises whenever the energy of photons interacting with the transition does not quite match up with the atomic transition energy. An intuitive picture of this process is proposed that naturally explains experimental findings. Moreover, quantitative analysis of the experimental data is discussed in detail. The results compare well with those from numerical simulations.

## II. THE SYSTEM

We consider a passive optical resonator filled with a nonlinear medium which consists of free atoms interacting with a cw light field and a static magnetic field. The experiment is accessible for a transparent theoretical description within a model involving three degrees of freedom. The system displays periodic and chaotic spin precession, and the cw character of the experiment makes it possible to take long streams of data so that a detailed analysis is feasible.

We use the $D_1$ line in sodium vapor, which usually has the complications of hyperfine splitting and Doppler broadening. A high buffer-gas pressure as used here simplifies the situation through overwhelming homogeneous line broadening. This allows a particularly transparent description in terms of the four-level scheme shown in Fig. 1. It is convenient to choose the direction of light propagation as quantization axis ($z$ axis). Left (right) circularly polarized light $\sigma_+$ ($\sigma_-$) will drive the transitions $1 \rightarrow 4$ ($2 \rightarrow 3$). Other states of polarization can be thought of as superpositions of $\sigma_+$ and $\sigma_-$. Driving just one transition creates, together with relaxation processes, a ground-state population difference $w$, which corresponds to an alignment of the spins and a result-

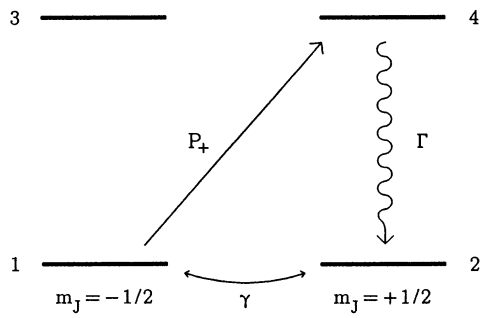


FIG. 1. Level scheme used to describe the $D_1$ transition in sodium. $\sigma_+$ light pumps the transition $1 \rightarrow 4$ with pump rate $P_+$. $\sigma_-$ light drives the transition $2 \rightarrow 3$ (not shown). Of all relaxation processes only the resulting net effects are shown with their relaxation rates $\Gamma$ and $\gamma$, respectively.

 ©1992 The American Physical Society

ing macroscopic magnetic moment in the probe. The pumping is counteracted by a much smaller decay rate $\gamma$ between the ground states (here $\gamma^{-1} = 10\ \mu$s, see Ref. [9]). $w$ saturates when the pumping rate due to the light intensity is comparable to $\gamma$.

This nonlinearity, in combination with optical feedback due to the resonator, gives rise to a variety of different instabilities. The first that has been observed [10] is optical bistability. In particular, absorptive bistability is obtained when the resonator is center tuned with respect to both the light and the atoms, whereas detuning leads to the dispersive counterpart. When both transitions are driven equally strong (linearly polarized input light), there is a competition between two pumping processes. In spite of the symmetry, one of the transitions will win out as the intensity is increased: a spontaneous symmetry breaking induces a switching to a finite $w$. This means high absorption for one component of the light, and low absorption for the other one. The result is nearly circularly polarized light in transmission. Since there are three possible states (linear, right circular, left circular), this effect is called tristability [11]. As with bistability, there exists a dispersive counterpart to the absorptive version just described, which can be understood in a completely analogous fashion: one polarization component is shifted into resonance with the cavity, the other is pushed away from it by virtue of intensity-dependent refractive indices.

Now assume that there is an external static magnetic field. First, consider the case of a transverse field (vanishing component along the $z$ axis). A new type of behavior appears: the aligned spins precess around the axis of this field. Thus, population is transferred to and fro between states 1 and 2. The precession frequency is essentially given by the Larmor frequency associated with the field strength. It has been shown that under conditions of optical feedback, in the dispersive case this spin precession is self-excited and self-sustaining [12]. As a consequence, the transmitted light will be modulated at the precession frequency.

This has been described in detail before in Ref. [9], where a good description was achieved with a theoretical model of three nonlinear coupled ordinary differential equations of first order ("3D model").

For our present purpose, one extension of this model is crucial. The inclusion of a longitudinal component of the external field leads to additional terms in the theoretical model which are essential for the generation of chaotic spin precession. This chaotic behavior is investigated in the present paper.

## III. EXPERIMENTS

This section starts with a presentation of the periodic oscillations in the case of a vanishing longitudinal field. Next, for a finite longitudinal field we show typical irregular oscillations and prove that they are deterministically chaotic.

The experimental setup is basically the same as in Ref. [9]. It is shown schematically in Fig. 2. Sodium vapor at a density of typically $10^{12}$–$10^{13}$ cm$^{-3}$ in an atmosphere of 200 mbar of argon buffer gas is placed inside a 150-mm near-confocal Fabry-Pérot resonator with "cold" finesse $F \approx 20$. The transmitted light is separated for its $\sigma_+$ and $\sigma_-$ components and detected by two photodiodes. The two signals are shown in Fig. 3 as traces (a) and (b). The oscillations are in opposite phase, as is to be expected, because at any one time the spins can be oriented only one way or the other, but not both.

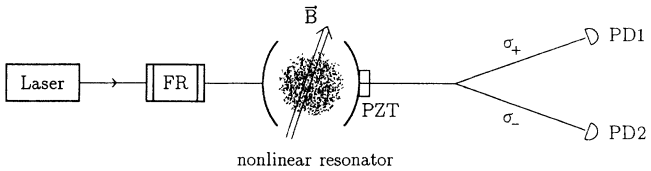


FIG. 2. Sketch of the experimental setup; some detail is omitted for clarity. A stabilized single mode cw dye ring laser is tuned near the $D_1$ resonance line of sodium. Reflections are suppressed by an optical diode, consisting of a 45° Faraday rotator (FR) and two polarizers. Mode matching and polarization optics create the desired beam characteristics and polarization state. The confocal sodium-filled resonator, surrounded by Helmholtz coils, has a cold finesse $F \approx 20$. Its length of about 150 mm is controlled with a piezoceramic translator (PZT) and servo locked to a frequency-stabilized He-Ne laser. The two polarization states of the transmitted beam are separated by a $\lambda/4$ plate and a Wollaston prism and are steered onto two equal photodiodes (PD1, PD2). Their signals are recorded with a two-channel 125-MHz LeCroy 9400 digital oscilloscope (32 000 data points per channel with eight-bit resolution).

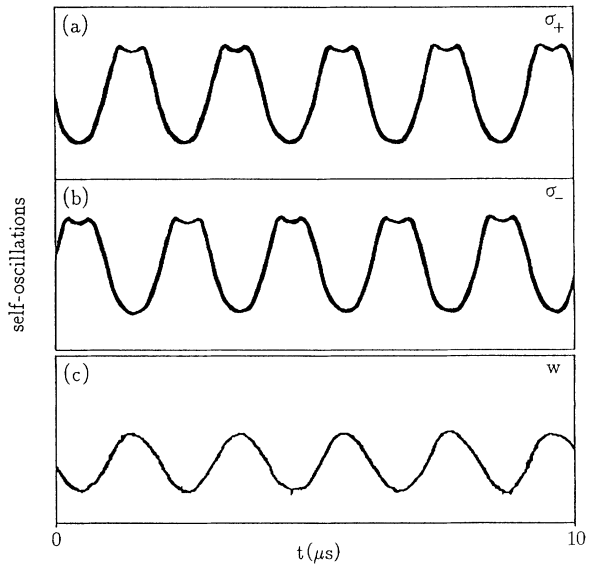


FIG. 3. Periodic self-oscillations: (a) transmitted intensity of the $\sigma_+$ light, (b) transmitted intensity of the $\sigma_-$ light, (c) transmitted probe beam ($\sim w$). Parameters: $P_{0-} = P_{0+} = 7$ mW, $B_x = 70\ \mu$T, $B_z = 0$, detuning 12 GHz, and buffer-gas pressure 200 mbar.

There is also a possibility to assess the ground-state population difference $w(t)$ directly. To this end, we employed custom-made resonator mirrors that were partially coated, and partially clear. This allowed us to send a separate light beam through the sodium vapor that made a small angle with respect to the primary beam and was not subject to resonator feedback. The probe beam was linearly polarized and therefore contained equal amounts of $\sigma_+$ and $\sigma_-$ light. These components experienced different phase shifts in the vapor. A second polarizer, set at 45° with respect to the incoming polarization, transformed the phase shifts into intensity variations which could be detected easily. With this technique, the temporal variation of $w$ could be seen directly [Fig. 3(c)]. $w(t)$ is found to vary almost sinusoidally, as is expected from the projection of a nearly circular precession motion. Whenever $w(t)$ is at a maximum, the intensity in $\sigma_-$ is high, and $\sigma_+$ is low. Just the opposite holds at the minima of $w(t)$. Note that the dips at the maxima of the transmitted intensities can now be understood easily: When $w(t)$ makes an excursion wide enough so that the shift in refractive index pushes either one of the polarization components beyond the cavity resonance, the corresponding intensity passes over the peak of the Airy function.

We now turn to the cases where more complicated types of oscillation were observed. In the experiments reported below, only the transmitted intensities were recorded for reasons of convenience. The correspondence between these and $w$ is established by Fig. 3 and Eq. (6) below. Typically the resonator phase, the irradiated intensity, and the magnetic field were varied. The transition from regular oscillation to chaos could occur along different routes [13]: Period doubling ($P1, P2, P4, \ldots, \chi$, where $\chi$ stands for chaos), quasiperiodicity ($P1$, torus, $\chi$), or intermittency ($P1$, bursts of $\chi$, $\chi$). Within the chaotic regime, periodic windows could be observed. It soon became clear from the experiment that chaos occurred under some very specific conditions.

(i) For chaos, the longitudinal component of the external magnetic field had to be within a suitable range.

(ii) Chaos occurred for purely circularly polarized light. It quickly disappeared as the polarization was made elliptic. There was no chaos at all with linear polarization.

(iii) Upon reversal of either the longitudinal field or the sense of circular polarization, chaos disappeared. It remained unchanged, however, if both were reversed.

An example of the observed chaotic oscillation is presented in Fig. 4. Panel (a) shows a section of the time series from a much longer data set. The envelope of the oscillation is irregularly modulated. The power spectrum (evaluated from the time series with a fast-Fourier-transform algorithm using a Blackman-Harris data window [14]) has a broad continuum predominantly at low frequencies, which is about 20 dB above the technical noise floor, and shows only mild peaking near the Larmor frequency [Fig. 4(b)].

A continuum as in Fig. 4(b) does not prove that the process is deterministically chaotic, since noise would have a continuous spectrum, too. The distinction between deterministic and stochastic signals relies on the detection of certain correlations in the signal. The most straightforward test, known as the first return map [15], deals with correlations of amplitudes of successive maxima. The return map is shown in Fig. 4(c). The points form a roughly arch-shaped curve, whereas an uncorrelated signal would give a featureless blob. It is therefore clear that the underlying process is deterministic. Similar arch-shaped curves are well known from the logistic map [16]. In distinction, however, here there is substructure in the main part of the arch, and a rising "tail" in the right part of the figure. Differences are not surprising, of course, because here we deal with a flow, rather than a 1D map.

The next step is to extract some quantitative information about the process from the recorded data. Since we have to work with noisy data sets of limited length, we restrict ourselves to well-established algorithms for the calculation of dimensions, entropies, and Lyapunov exponents, the limitations and potential pitfalls of which are fairly well studied [17–19]. For example, it is known that noise reduction through low pass filtering yields a systematic error for the dimension estimate [20–22]. Acausal filters were used to avoid that problem [23], but here they did not provide a substantial benefit because noise occurred predominantly at low frequencies. Therefore, the data presented in this paper are unfiltered.

Since only one variable was recorded, we first have to reconstruct the attractor through the well-known time-delay technique [24]. Its portrait is shown in Fig. 4(d). The correlation dimension $D_2$ of the attractor and the related entropy $K_2$ were determined with an algorithm proposed by Grassberger and Procaccia [25]. Figure 5 shows the result of one such calculation of the slope of the correlation integral. The average over the scaling region as a function of the embedding dimension (see Fig. 6) converges to what we consider a preliminary dimension estimate. We tested this estimate through variation

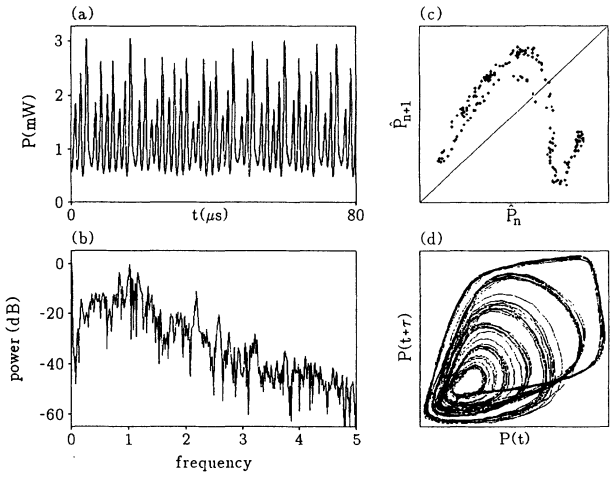


FIG. 4. Chaotic signal: (a) part of the time series (8000 of 32 000 points shown), (b) power spectrum, frequency in units of inverse mean orbital period, (c) return map, and (d) reconstructed attractor. Parameters: $P_{0+} = 20$ mW, $P_{0-} = 0$, $B_x = 38$ $\mu$T, $B_z = 102$ $\mu$T, and detuning 32.2 GHz.

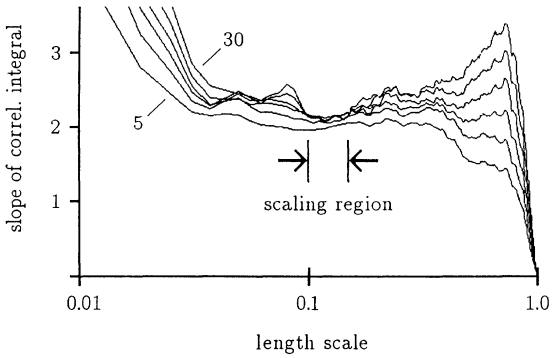


FIG. 5. Slope of the correlation integral vs length scale for embedding dimensions 5 to 30 in steps of 5. An interval from 0.10 to 0.15 was chosen as the scaling region. The length scale is normalized to the largest distance. In this example, every fourth point from the 32 000-point data set was selected as a first coordinate for the reconstruction of attractor points, and the delay between two successive coordinates was eight points.

of the sample size (number of points) and the two delay parameters involved in the time-delay embedding technique. The resulting average and scatter of dimension estimates were used as a final estimate and an indication for the error margins of the computation. The data set discussed here yields $D_2 = 2.12 \pm 0.03$. By a similar procedure we evaluate its correlation entropy and find $K_2 = (7 \pm 1)\gamma$.

To clearly discern chaotic from stochastic structure we used the technique of surrogate data [17, 26]. It compares the dimension estimate for the original data with those for randomized data, obtained by first scrambling the phases of the Fourier transform of the original, then transforming back to the time domain. As there was no plateau in the slope of the correlation integral for the surrogates (as expected for random signals), the same scaling region as for the original data was used throughout. The shaded area in Fig. 6 indicates the mean value plus or minus one standard deviation of the dimension estimate for a set of ten surrogates. The difference between original and surrogates is statistically significant: on average from embedding dimension 5 to 40, it amounts to 14 standard deviations.

We never obtained data for which $D_2 \geq 3$ (typically, $D_2 \approx 2.1$), and therefore proceed on the assumption that a 3D model suffices to describe the system. Results below will further justify this approach.

A 3D system is characterized by three Lyapunov exponents. In case of nonstationary dynamics one of these ($\lambda_0$) is zero by necessity [27], one is positive to allow for chaos ($\lambda_+$), and one is negative for energy dissipation ($\lambda_-$). We used an algorithm presented by Wolf *et al.* [28]. It evaluates the largest positive Lyapunov exponent from a time series because it is sensitive to the direction of strongest divergence of neighboring trajectories [29]. We have found that one can also use the same algorithm to determine the most negative Lyapunov exponent by using the attractor points in reverse temporal order. Through temporal inversion, diverging trajectories become converging and vice versa. We have tested this procedure on data with known exponents [30] and found that it gives correct results if the algorithm converges well for $\lambda_+$ and if $\lambda_+$ and $|\lambda_-|$ are not different by more than one order of magnitude. In a 3D system, the complete Lyapunov spectrum is thus determined. The error margins for the computation are again checked through variation of the computational parameters and we find $\lambda_+ = K_1 = (8.1 \pm 0.8)\gamma$ and $\lambda_- = (-75 \pm 10)\gamma$.

The computations presented so far can be checked for mutual consistency. One test is a comparison of $\lambda_+$ with the entropy $K_2$, since $\lambda_+ = K_1 \geq K_2$ [31]. Another one is whether $D_2 \leq D_1$, where $D_1$ is obtained from the Kaplan-Yorke formula, which gives the dimension $D_1$ as a function of the Lyapunov exponents [31]. For our 3D system, it reads

$$D_1 = 2 + \lambda_+/|\lambda_-|. \tag{1}$$

Here we find $D_1 = 2.11 \pm 0.02$. In view of the numerical uncertainties, the agreement is very satisfactory. Still another test is less suitable for experimental data but will be applied to numerical results below: The sum of all Lyapunov exponents has to be equal to the phase-space contraction rate which can be obtained from a model.

We thus get from one data set, through independent algorithms, characteristic values that have to obey specific relations. They do, and we are therefore confident that

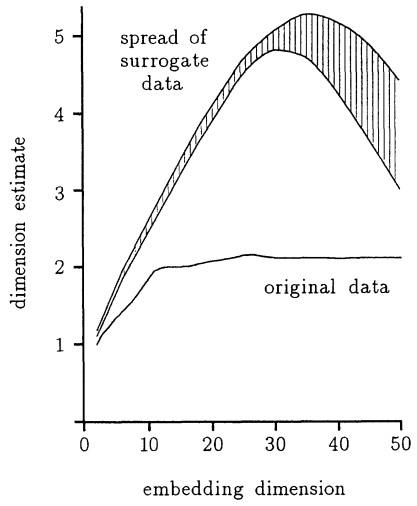


FIG. 6. Dimension estimate for the original data set and the surrogate data as a function of the dimension of the embedding space. The original data set of 32 000 points was compressed to $2^{13}$ points by taking every third point. The phases of its Fourier transform were then replaced with sets of random numbers equally distributed in $[0; 2\pi]$. By inverse Fourier transformation a total of ten surrogate data sets was generated. For these and the compressed data set, dimension estimates were calculated from the same scaling region using all points and a delay of two between the components for the attractor reconstruction, respectively. The shaded area indicates an interval of $\pm 1$ standard deviations around the average of these dimension estimates.

they quantify the observed dynamics correctly within the error margins stated. Generally, we feel that calculations of dimensions, etc., should never be considered reliable unless such checks have been made.

## IV. THEORETICAL MODEL

The time evolution of our system can be described semiclassically by the equation of motion for the density matrix $\rho$:

$$i\hbar\dot{\rho} = [H, \rho] + \text{relaxation terms}. \tag{2}$$

A detailed derivation of the model for the case with a purely transverse magnetic field has been given in Ref. [9]. Therefore, only a brief review is given here, with an emphasis on the modifications required for an arbitrary direction of the magnetic field.

We write the Hamiltonian in the form $H = H_0 + H_E + H_B$, with $H_0$ for the free atom, and $H_E$ and $H_B$ for the interaction with the light field and the magnetic field, respectively. The light field is described as a monochromatic plane wave of the form

$$E(z,t) = \tfrac{1}{2}[E_+(z)(\mathbf{e}_x + i\mathbf{e}_y) + E_-(z)(\mathbf{e}_x - i\mathbf{e}_y)]e^{-i\omega t} + \text{c.c.}, \tag{3}$$

where $E_+$ and $E_-$ are the amplitudes of the circularly polarized light field components $\sigma_+$ and $\sigma_-$.

This leads to the following elements in the Hamiltonian:

$$\begin{aligned}
H_{11} &= \hbar(\omega_1 - \tfrac{1}{2}\Omega_z),\\
H_{33} &= \hbar(\omega_3 - \tfrac{1}{2}\Omega_z),\\
H_{22} &= \hbar(\omega_1 + \tfrac{1}{2}\Omega_z),\\
H_{44} &= \hbar(\omega_3 + \tfrac{1}{2}\Omega_z),\\
H_{21} &= H_{43} = -\frac{\hbar}{2}(\Omega_x + i\Omega_y),\\
H_{31} &= H_{42} = 0,\\
H_{32} &= \hbar(\beta_- e^{-i\omega t} + \beta_+^* e^{i\omega t}),\\
H_{41} &= \hbar(\beta_+ e^{-i\omega t} + \beta_-^* e^{i\omega t}).
\end{aligned}$$

Here, $\hbar\omega_1$ and $\hbar\omega_3$ denote the unperturbed energies of the atomic levels 1 and 3, and $\omega_0 = \omega_1 - \omega_3$ is the corresponding atomic transition frequency. $\beta_\pm = \mu_E E_\pm/2\hbar$ denote the electric dipole coupling strengths for the $\sigma_\pm$ components, and $\mu_E$ is the reduced electric dipole matrix element. $\Omega_x$, $\Omega_y$, and $\Omega_z$ are the three spatial components of the external magnetic field $\mathbf{B}$, normalized as Larmor frequencies through $\Omega_i = \mu_B g_J B_i/\hbar$. The relaxation terms are introduced phenomenologically and remain the same as in Ref. [9].

In the calculation, excited-state population is neglected. This is a valid approximation as long as the intensities are relatively low. Extensions of the model have been given to cover higher intensities [32], but for the present purposes we need not be concerned with that. Within the rotating-wave approximation and after adiabatic elimination of the coherences involving the excited states, we obtain a description in which only the two sublevels of the ground state are relevant for the dynamics. The spin orientation in the ground state has the value $\mathbf{m} = (u, v, w) \in \mathbb{R}$, where

$$u = \rho_{12} + \rho_{21}, \quad v = i(\rho_{12} - \rho_{21}), \quad w = \rho_{11} - \rho_{22}.$$

The equation of motion for $\mathbf{m}$ is given by

$$\dot{\mathbf{m}} = -(\gamma + S)\mathbf{m} + \mathbf{T} + \mathbf{m} \times \mathbf{\Omega}, \tag{4}$$

with $\mathbf{\Omega} = (\Omega_x, \Omega_y, \Omega_z - D\Delta)$, and $\mathbf{T} = (0, 0, D)$. As mentioned above, $\gamma$ is the relaxation rate between the substates of the ground state. $\Delta$ is the detuning $(\omega_0 - \omega)/\Gamma$, with $\Gamma$ the decay rate of the optical coherence. $S = P_+ + P_-$ and $D = P_- - P_+$, where

$$P_\pm = \frac{1}{\Gamma}\frac{|\beta_\pm|^2}{\Delta^2 + 1} \tag{5}$$

are the normalized intensities, or pumping rates, for the right and left circularly polarized light field components inside the resonator. Since the description was effectively reduced to a two-level system, it is no surprise [33] that the resulting equation of motion formally resembles the well-known Bloch equation [34].

The optical feedback is represented mathematically through the resonator equation (written here for a ring resonator for simplicity)

$$P_\pm(w) = \frac{P_{0\pm}(1 - R_f)}{1 + (\mathrm{Re}^{-\alpha L(1\pm w)})^2 - 2\,\mathrm{Re}^{-\alpha L(1\pm w)}\cos(\pm\Phi_1 w - \Phi_0)}. \tag{6}$$

$P_{0\pm}$ describes the incoming intensity for the two light field components and $R = \sqrt{R_f R_b}$ is the effective reflectivity of the front and back resonator mirrors $R_f$ and $R_b$. $\alpha$ is the intensity absorption coefficient of the sodium vapor at the laser frequency, and $L$ the interaction length. $\Phi_1$ is given by $(n-1)\omega L/c$, where $n$ is the small signal refractive index. Through dispersion relations, $\Phi_1 = \alpha\Delta$. $\Phi_0$ is the resonator round trip phase at low intensity.

Equations (4) and (6) together constitute our model. It is instructive to understand the physical meaning of the individual terms. Equation (6) is the well-known Airy function, except for the exponential functions in the denominator, which describe nonlinear absorption, and the nonlinear phase shift $\pm\Phi_1 w$ contained in the cosine. Note that all the nonlinearity of the problem comes from these terms. The first term on the right-hand side (RHS) of Eq. (4) describes the dissipation of energy to the heat bath. The second term stands for an energy supply from the photons to the spin system; this term drives the system out of equilibrium and is responsible, e.g., for bistability in the absence of magnetic fields. The last term on the RHS of Eq. (4) describes the precession of $\mathbf{m}$ around

$\Omega$ as the external magnetic field exerts torque on the atomic magnetic moments. Note that $\Omega$ also contains an intensity-dependent term $D\Delta$ by which the photons can supply energy to the precession.

This term merits further discussion. Atomic levels in the presence of a light field are energetically shifted; this is well known under the names "ac Stark shift" or "light shift." It has been described in detail in Ref. [35] and references therein. In our case, sublevel 1 is shifted in proportion to $P_+\Delta$, and 2 is shifted in proportion to $P_-\Delta$. The degeneracy of the substates is thus lifted by a net shift $D\Delta$. The light shift can also be interpreted as a fictitious magnetic field [35]. Accordingly it appears here in sum with the component $\Omega_z$ of the magnetic field, which also lifts the degeneracy through Zeeman splitting.

A first qualitative test of our model is whether symmetries of the model reflect the experimental findings. Simultaneous reversal of $D$ and $\Omega_z$ (i.e., $\sigma_+ \rightarrow \sigma_-$ and $\Omega_z \rightarrow -\Omega_z$) does not change the absolute value of the term $(\Omega_z - D\Delta)$. One therefore expects unchanged behavior, except for a different sense of precession. This is in agreement with experimental observation, as was pointed out above. The model also suggests that a reduction of $D$ can be compensated for through an increase in $\Delta$ to retain the same dynamic behavior. Similarly, small changes in $D$ can, within limits, be accounted for through compensating changes in $\Omega_z$. This was confirmed in the experiment as well. We also find that larger changes in $\Omega_z$ can only be compensated for when $\Omega_x$ or $\Omega_y$ are also changed roughly in proportion such that the spatial direction of the resulting magnetic field is kept approximately constant. This is plausible by the following argument: The three equations for $\dot{u}$, $\dot{v}$, and $\dot{w}$ implicit in Eq. (4) are linked by coupling terms of comparable order of magnitude. With said compensating changes the ratio of these terms remains essentially unchanged.

## V. NUMERICAL SIMULATIONS

In the numerical simulation we choose $\sigma_+$ light and, due to cylindrical symmetry around the $z$ axis, omit $\Omega_y$ without loss of generality. Also we normalize $P_{0+}$, $\Omega_x$, $\Omega_z$, and time to units of $\gamma^{-1}$. We thus deal with a seven-dimensional parameter space spanned by $P_{0+}$, $\alpha L$, $\Phi_0$, $\Delta$, $\Omega_x$, $\Omega_z$, and $R$ [36].

The corresponding experimental parameters are known. Unfortunately, for $\Phi_0$, on which the behavior is very critically dependent, we did not achieve sufficient accuracy. For $P_{0+}$, there is a conceptual problem: The model assumes plane waves, whereas in the experiment there is a transverse beam profile (the shape of which, given a nonlinear absorber, has to be neither Gaussian nor even constant in time). Therefore, the corresponding $P_{0+}$ is known only in coarse approximation.

In locating a chaotic regime numerically, we benefitted from calculations by Lange, Nalik, and Möller [37] on a similar model that also included the excited-state population as an additional variable and was thus four dimensional. With the help of the AUTO software package [38] they found parameter sets for chaos; starting from one of these sets we found qualitatively similar chaos in our 3D model also. Thus, at least the existence of chaos in the 3D model was proven, and while details may differ and the chaotic regime may be larger in 4D, the mechanism must be all there in the 3D model.

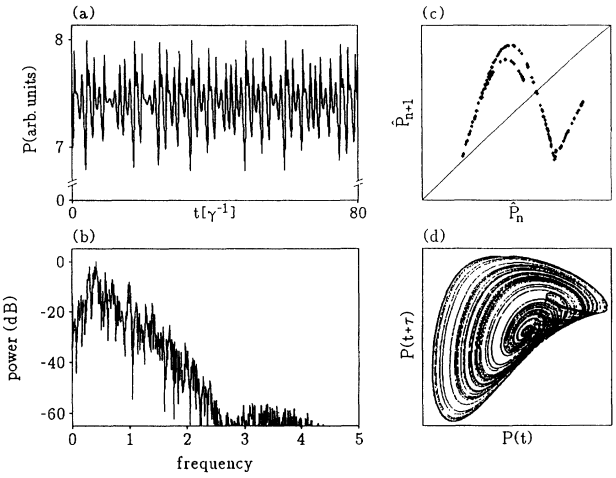


FIG. 7. Chaotic signal from a numerical simulation: (a) part of the time series (8000 of 32 000 points shown), (b) power spectrum, frequency in units of inverse mean orbital period, (c) return map, and (d) reconstructed attractor. Parameters: see Table I.

Figure 7 shows a result from numerically simulated chaos in the 3D model. The magnetic fields chosen here are smaller than what would correspond to the experiment, a difference in which the main effect has simply been a change of the oscillation frequency. The other parameters are realistic for comparison with the experiment, but in view of the above-mentioned difficulties we cannot claim exact correspondence. It is therefore encouraging that a comparison of results from computation and experiment reveals a lot of similarity between both. Analysis of the attractor shown here, using the same algorithms as for the experimental data, yielded $D_2 = 2.07$, $K_2 = 0.62\gamma$, $\lambda_+ = 0.76\gamma$, and $\lambda_- = -11.4\gamma$. Applying the cross checks mentioned above we find that indeed $K_2 \leq \lambda_+$ and $D_1 = 2.07 \geq D_2$, and that $\lambda_+ + \lambda_- = -10.6\gamma$, to be compared to the average phase-space contraction rate $\langle \partial\dot{u}/\partial u + \partial\dot{v}/\partial v + \partial\dot{w}/\partial w \rangle = -9.4\gamma$. Again these cross checks give mutually consistent results. Furthermore, experimental and numerical data show reasonable agreement considering the different time scales mentioned above. Beyond this analysis we found both the period-doubling route and the quasiperiodicity route to chaos also seen in the experiment. Table I gives representative parameter values.

## VI. REDUCTION OF THE MODEL

It could be shown so far in this paper that our 3D model is indeed able to describe deterministic chaos in qualitative agreement with the experimental results. Beyond that, one may ask what the physical mechanism is that drives the system from periodic self-oscillations into

TABLE I. Parameter values for the numerical simulation [Eqs. (4) and (6)], which produce (a) the chaotic behavior shown in Fig. 7, (b) a period-doubling sequence or (c) a torus followed by chaos through the variation of the pump intensity, and (d) gives parameters for chaos in the reduced model with a linearized $\mathbf{T}$ of the form $\mathbf{T} = (-1.9w, 0, -0.1)$. In all cases $R_f = R_b = R$.

| Scenario | $P_{0+}$ | $\Phi_0$ | $\Omega_x$ | $\Omega_z$ | $\Delta$ | $\alpha L$ | $R$ |
|---|---|---|---|---|---|---|---|
| (a) $\chi$ of Fig. 7 | 0.2292 | −0.635 | −24.25 | −48.0 | 31 | 0.1 | 0.9322 |
| (b) Period doubling | 0.196–0.2292 | −0.635 | −24.25 | −48.0 | 31 | 0.1 | 0.9326 |
| (c) Torus | 0.354–0.360 | −0.570 | −21.5 | −43.0 | 31 | 0.06 | 0.9326 |
| (d) $\chi$ (reduced model) | 0.109 86 | −3.1128 | −37.46 | −56.5 | 38 | 0.1005 | 0.9450 |

chaos. Since chaotic behavior arises from nonlinearities, the question is whether any of the nonlinear terms in Eq. (4) can be identified as the crucial one.

We opted for the approach of eliminating the nonlinear terms one by one by replacing them with linear or even constant terms to determine whether the chaotic behavior is maintained, possibly through slight changes in the remaining parameters.

As noted above, the nonlinearity in the problem is entirely contained in $P_+ = P_+(w)$ as given by Eq. (6). There is both a nonlinear phase shift (in the cosine) and nonlinear absorption (in the exponential functions). If the latter are replaced by the constant $\mathrm{Re}^{-\alpha L}$, chaos persists. We therefore deal here with a purely dispersive effect relying on the nonlinear phase shift.

In Eq. (4), $P_+(w)$ apears in three places. In the dissipative term $-[\gamma + P_+(w)]\mathbf{m}$, it can be simply set to zero, and chaos still persists. In $\mathbf{T}$, it can be replaced by a linear function of $w$. This leaves us with $\mathbf{\Omega}$, where the third component reads $\Omega_z - P_+(w)\Delta$. The light shift term alone is thus capable of generating chaos in our model. The question arises whether any of the other nonlinear terms has the same property.

This can be addressed as follows. All routes to chaos discussed above start with a Hopf bifurcation from steady-state to self-oscillating behavior. In the model, further characterization of this bifurcation is possible; it turned out that it consistently occurred for $\partial P_+(w)/\partial w > 0$, independently of the above eliminations. However, if the $P_+(w)\Delta$ term is replaced by a constant, it can be shown analytically that Hopf bifurcations are no longer possible on this branch. The proof is given in the Appendix. Therefore, the routes to chaos discussed here cannot occur without the light shift term. The light shift $P_+(w)\Delta$ is thus singled out as the nonlinear term necessary and sufficient for deterministic chaos in our system.

With this knowledge we can give an intuitive picture of the process that allows the onset of chaotic behavior in our system. The term $\mathbf{m} \times \mathbf{\Omega}$ in Eq. (4) describes the precession of the magnetization $\mathbf{m}$ around the axis of the effective magnetic field $\mathbf{\Omega}$. Neither magnitude nor spatial direction of $\mathbf{\Omega}$ are constant, rather both are $w$ dependent: the angular velocity of the precession, e.g., is given by $|\mathbf{\Omega}| = [\Omega_x^2 + \Omega_y^2 + (\Omega_z - D\Delta)^2]^{1/2}$. It is modulated with $D\Delta$.

As a specific example, let $P_+$ oscillate periodically and choose $D = -P_+$, $\Delta > 0$, $\Omega_z < 0$, and $|\Omega_z| > |P_+\Delta|$ at all times. At times when the population is at its minimum in 1 and at its maximum in 2, the absorption is at a minimum. Thus, $P_+$ assumes its maximum value. During the half cycle in which the atoms go from state 2 to state 1, $P_+$ decreases. Since $(\Omega_z + P_+\Delta)^2$ has the opposite phase of $P_+$ alone, $|\mathbf{\Omega}|$ increases: the precession is accelerated. During the other half cycle, it is decelerated. However, during this half cycle the atoms have an additional channel from 1 to 2 through optical pumping via 4. Thus the acceleration is "in phase" with the precession in the sense that it affects all the spins, whereas only a smaller number of preceding spins is decelerated. For $\sigma_-$ light, on the other hand, there is a net deceleration.

From this it becomes clear that the light shift provides a nonlinear feedback, acting on the axis and the velocity of the spin precession. It can either feed energy into the precession or absorb energy from it. For linear polarization, the situation is symmetric with respect to optical pumping, and the net effect on the precession is nil.

Going back now to the conditions (i)–(iii) for chaos in the experiment given above, one immediately sees a remarkable correspondence: The experiment shows chaos if and only if the intuitive picture indicates "in phase" feedback.

We thus visualize the generation of chaos as follows. A nonlinear feedback, mediated by the light shift, perturbs the regular precession. If the perturbation is in phase and strong enough (e.g., as one raises the input power $P_{0+}$), the periodic precession is destabilized. This is the onset of chaos.

## VII. SUMMARY

We have shown that spin-$\frac{1}{2}$ atoms in an optical resonator can, in addition to other instabilities observed before, exhibit deterministic chaos. Our experimental data allowed a detailed quantitative analysis of the dynamics. The results for attractor dimension, Lyapunov exponents, and entropy pass the test of mutual cross checks. A previous theoretical model consisting of three differential equations, modified to cover the present case, is capable of producing chaos with many characteristics that are also observed in the experiment.

Rather than perfecting this model through inclusion of more detail, we went the opposite way and simplified it by linearizing nonlinear terms such that chaos still persisted. In the end, only a term describing the light shift of the participating atomic levels turned out to be necessary. Since chaos can never occur in linear systems, this must

be the nonlinear term responsible for chaos. An intuitive picture is suggested of how the light shift perturbs the regular motion and leads into chaos.

## ACKNOWLEDGMENTS

We thank W. Lange, J. Nalik, and M. Möller for frequent fruitful discussions and exchange of information. R. Deserno participated in the measurements connected with Fig. 3. Partial support by the Commission of the European Communities is gratefully acknowledged.

## APPENDIX

The numerical simulations have shown that a reduced theoretical model containing the light shift $-P_+\Delta$ as the only nonlinear term is still able to produce chaos similar to that obtained from the complete model. For all cases the chaotic behavior was preceded by a Hopf bifurcation which occurred in the regime of $P'_+ = \partial P_+/\partial w > 0$. Assume that there is some other reduction that keeps this characteristic of the transition but involves elimination of the light shift. First replace $(\Omega_z - P_+\Delta)$ in Eq. (4) with $\Omega_z$ to linearize $\mathbf{m}\times\mathbf{\Omega}$. This leads to a simplified system of three scalar equations. The eigenvalues $\lambda$ of its Jacobian are solutions of the following characteristic equation:

$$0 = -\lambda^3 - \lambda^2[3(1+P_+) + P'_+(1+w)] - \lambda[3(1+P_+)^2 + 2P'_+(1+P_+)(1+w) - P'_+\Omega_x v + \Omega_x^2 + \Omega_z^2] - (1+P)^3$$
$$-(1+P)(\Omega_x^2 + \Omega_z^2 - \Omega_x P'_+ v) - P'_+[(1+w)(1+P_+)^2 - u\Omega_x\Omega_z + \Omega_z^2(1+w)].$$

At a Hopf bifurcation, two of these eigenvalues have to be purely imaginary, i.e., $\lambda_\pm = \pm i\phi$ with $\phi \in \mathbf{R}\backslash\{0\}$. We thus insert $i\phi$ for $\lambda$. Since this equation has to hold for its real and imaginary part simultaneously, $\phi$ can be eliminated. This yields the following necessary condition for the existence of a Hopf bifurcation:

$$0 = 8(1+P_+)^3 + 2(1+P_+)(\Omega_x^2 + \Omega_z^2) + P'^2_+(1+w)[2(1+P_+)(1+w) - v\Omega_x]$$
$$+P'_+[8(1+w)(1+P_+)^2 + \Omega_x^2(1+w) - 2v\Omega_x(1+P_+) - u\Omega_x\Omega_z]. \quad \text{(A1)}$$

Since by definition $P_+ \geq 0$, $(1+w) \geq 0$, and in the case considered here also $P'_+ > 0$, all terms except the ones containing $v\Omega_x$ or $u\Omega_x\Omega_z$ are thus immediately seen to be positive. The signs of the latter follow from the steady-state condition $\dot{\mathbf{m}} = \mathbf{0}$, which yields

$$u = \frac{\Omega_x\Omega_z}{\Omega_z^2 + (1+P_+)^2} w, \quad \text{(A2)}$$

$$v = \frac{\Omega_x(1+P_+)}{\Omega_z^2 + (1+P_+)^2} w, \quad \text{(A3)}$$

$$P_+(w) = -(1+P_+)\left(\frac{\Omega_x^2}{\Omega_z^2 + (1+P_+)^2} + 1\right) w. \quad \text{(A4)}$$

Equation (A4) requires $w \leq 0$. With this, Eqs. (A2) and (A3) yield $v\Omega_x \leq 0$ and $u\Omega_x\Omega_z \leq 0$. Therefore, all terms on the RHS of Eq. (A1) are positive, and Eq. (A1) has no solution. We conclude that in the absence of the light shift term, a Hopf bifurcation does not exist for $\partial P_+/\partial w > 0$. Hence, the light shift is necessary for the type of chaos reported here.

[1] H. G. Schuster, *Deterministic Chaos* (VCH Verlagsgesellschaft, Weinheim, 1989).
[2] *Measures of Complexity and Chaos*, edited by N. B. Abraham, A. M. Albano, A. Passamante, and P. E. Rapp (Plenum, New York, 1989).
[3] P. W. Milonni, M. L. Shih, and J. R. Ackerhalt, *Chaos in Laser-Matter Interactions* (World Scientific, Singapore, 1987).
[4] L. M. Narducci and N. B. Abraham, *Laser Physics and Laser Instabilities* (World Scientific, Singapore, 1988).
[5] Topical issue on nonlinear dynamics of lasers, J. Opt. Soc. Am. B **5**, 876 (1988).
[6] *Instabilities and Chaos in Quantum Optics II*, edited by N. B. Abraham, F. T. Arecchi, and L. A. Lugiato (Plenum, New York, 1988).
[7] *Optical Chaos*, edited by J. Chrostowski and N. B. Abraham, SPIE Proceedings Vol. 667 (SPIE, Bellingham, 1986).
[8] *OSA Proceedings on Nonlinear Dynamics in Optical Systems*, edited by N. B. Abraham, E. M. Garmire, and P. Mandel (Optical Society of America, Washington, DC, 1991), Vol. 7.
[9] F. Mitschke, R.Deserno, W. Lange, and J. Mlynek, Phys. Rev. A **33**, 3219 (1986).
[10] J. Mlynek, F. Mitschke, R. Deserno, and W. Lange, Phys. Rev. A **29**, 1297 (1984).
[11] M. Kitano, T. Yabuzaki, and T. Ogawa, Phys. Rev. Lett. **46**, 926 (1981).
[12] M. Kitano, T. Yabuzaki, and T. Ogawa, Phys. Rev. A **24**, 3156 (1981).
[13] J. P. Eckmann, Rev. Mod. Phys. **53**, 643 (1981).
[14] F. J. Harris, Proc. IEEE **66**, 51 (1978).
[15] E. N. Lorenz, J. Atmos. Sci. **20**, 130 (1963).
[16] M. J. Feigenbaum, J. Stat. Phys. **19**, 25 (1978).
[17] J. Theiler, Phys. Lett. A **155**, 480 (1991).
[18] See, e.g., several contributions in *Dimensions and Entropies*, edited G. Mayer-Kress (Springer-Verlag, Berlin, 1986).
[19] M. Möller, W. Lange, F. Mitschke, N. B. Abraham, U. Hübner, Phys. Lett. A **138**, 176 (1989).

[20] R. Badii and A. Politi, in *Dimensions and Entropies*, edited by G. Mayer-Kress (Springer-Verlag, Berlin, 1986), p. 67.
[21] F. Mitschke, M. Möller, and W. Lange, Phys. Rev. A **37**, 4518 (1988).
[22] R. Badii, G. Broggi, B. Derighetti, M. Ravani, S. Ciliberto, A. Politi, and M. A. Rubio, Phys. Rev. Lett. **60**, 979 (1988).
[23] F. Mitschke, Phys. Rev. A **41**, 1169 (1990); F. Mitschke and M. Dämmig, in *OSA Proceedings on Nonlinear Dynamics in Optical Systems*, edited by N. B. Abraham, E. M. Garmire, and P. Mandel (Optical Society of America, Washington, D.C. 1991), Vol.7.
[24] F. Takens, in *Dynamical Systems and Turbulence*, edited by D. A. Rand and L.-S. Young, Lecture Notes in Mathematics Vol. 898 (Springer-Verlag, Berlin, 1981).
[25] P. Grassberger and I. Procaccia, Physica **9D**, 189 (1983).
[26] J. Theiler, B. Galdrikian, A. Longtin, S. Eubank, and J. D. Farmer, in *Nonlinear Modeling and Forecasting*, edited by M. Casdagli and S. Eubank, Vol. XII of *SFI Studies in the Sciences of Complexity* (Addison-Wesley, Reading, MA, 1992), pp. 163–188.
[27] H. Haken, Phys. Lett. **94A**, 271 (1983).
[28] A. Wolf, J. B. Swift, H. L. Swinney, and J. A. Vastano, Physica **16D**, 285 (1985).
[29] The widely held belief that noise gives rise to a Lyapunov exponent of infinite value is wrong: that applies only to $\delta$-correlated noise, which is not typically encountered in experiments. Even for random data, the calculation converges to a finite result, which seems to be determined by the signal's correlation time. Surely, even for noise that is white on the time scales considered, a computation of averages from a finite set of bounded numbers will always produce a convergent, finite result.
[30] We used the Rössler model with parameter values as in Ref. [28] and the system described in F. Mitschke, M. Möller, and W. Lange, Phys. Rev. A **37**, 4518 (1988).
[31] P. Grassberger and I. Procaccia, Physica **13D**, 34 (1984).
[32] J. Nalik, W. Lange, and F. Mitschke, Appl. Phys. B **49**, 191 (1989).
[33] R. P. Feynman, F. L. Vernon, Jr., and R. W. Hellwarth, J. Appl. Phys. **28**, 49 (1957).
[34] F. Bloch, Phys. Rev. **70**, 460 (1946).
[35] C. Cohen-Tanoudji and Jacques Dupont-Roc, Phys. Rev. A **5**, 968 (1972).
[36] For $R$ we have to use $(R_{\text{measured}}+1)/2$ to account for the fact that the experiment takes place in a Fabry-Pérot resonator, whereas Eq. (6) is valid for a ring resonator.
[37] W. Lange, J. Nalik, and M. Möller (private communication).
[38] E. Dödel, Congr. Numer. **30**, 265 (1981).